Hydrological Sciences Journal

ISSN: 0262-6667 (Print) 2150-3435 (Online) Journal homepage: https://www.tandfonline.com/loi/thsj20

Large-scale climate teleconnections with South Korean streamflow variability

Jai Hong Lee, Pierre Y. Julien, Christopher Thornton & Chang Hae Lee

To cite this article: Jai Hong Lee, Pierre Y. Julien, Christopher Thornton & Chang Hae Lee (2019): Large-scale climate teleconnections with South Korean streamflow variability, Hydrological Sciences Journal, DOI: 10.1080/02626667.2019.1617869

To link to this article: https://doi.org/10.1080/02626667.2019.1617869

Published online: 31 Oct 2019.

HYDROLOGICAL SCIENCES JOURNAL
https://doi.org/10.1080/02626667.2019.1617869

Large-scale climate teleconnections with South Korean streamflow variability

Jai Hong Lee[a], Pierre Y. Julien[b], Christopher Thornton[b] and Chang Hae Lee[c]

[a]Department of Civil and Mechanical Engineering, South Carolina State University, Orangeburg, South Carolina, USA; [b]Department of Civil and Environmental Engineering, Colorado State University, Fort Collins, Colorado, USA; [c]Division of Energy and Environmental Engineering, Daejin University, Pocheon-Si, Gyeonggi-Do, Republic of Korea

ABSTRACT

Leading patterns of observed seasonal extreme and mean streamflow on the Korean peninsula were estimated using an empirical orthogonal teleconnection (EOT) technique. In addition, statistical correlations on a seasonal basis were calculated using correlation and regression analyses between the leading streamflow patterns and various climate indices based on atmospheric–ocean circulation. The spatio-temporal patterns of the leading EOT modes for extreme and mean streamflow indicate an upstream mode for the Han River, with increasing trends in summer, and a downstream mode for the Nakdong River, with oscillations mainly on inter-decadal time scales in winter. The tropical ENSO (El Niño Southern Oscillation) forcing for both extreme and mean streamflow is coherently associated with summer to winter streamflow patterns. The western North Pacific monsoon has a negative correlation with winter streamflow variability, and tropical cyclone indices also exhibit significant positive correlation with autumn streamflow. Leading patterns of autumn and winter streamflow time series show predictability up to two seasons in advance from the Pacific sea-surface temperatures.

ARTICLE HISTORY
Received 28 August 2018
Accepted 28 March 2019

EDITOR
A. Castellarin

ASSOCIATE EDITOR
W. Collischonn

KEYWORDS
streamflow variability; El Niño Southern Oscillation (ENSO); teleconnection

Introduction

Overall, the river basins in the Korean peninsula experience spatial and temporal streamflow variability. Streamflow variation is related to fluctuations of various climate indices (CIs) representing large-scale climate phenomena, including El Niño, La Niña, Southern Oscillation, tropical cyclone and monsoon activity. These large-scale climate signals have been widely studied on global and regional scales, since the climatic impacts are associated with hydro-climatic extreme events, i.e. floods, droughts or abnormal heat wave, throughout the world. At various scales, significant findings have been investigated for teleconnections of the large-scale CIs and hydro-meteorological variables, including streamflow, precipitation and temperature (Douglas and Englehart 1981, Ropelewski and Halpert 1986, 1989, Kiladis and Diaz 1989, Kahya and Dracup 1994, Karabörk and Kahya 2003, Jin *et al.* 2005, Lee *et al.* 2005, Chandimala and Zubair 2007, Maity and Kashid 2010).

The El Niño Southern Oscillation (ENSO) index has been widely reported as a climatic indicator having an effect on hydro-meteorological variability at both regional and global scales. Since the first studies on the climatic relationship between the Southern Oscillation (SO) and the Indian monsoon rainfall variability (Walker 1923, Walker and Bliss 1932), many global-scale investigations into ENSO remote forcing have revealed notable teleconnection between various hydro-climatic parameters and the extreme phases of ENSO in many areas throughout the globe. Ropelewski and Halpert (1986, 1989) showed statistically significant ENSO-related climate signals by detecting the spatio-temporal scopes having a consistent and coherent impact of the extreme phases of the ENSO phenomenon on the precipitation and temperature pattern in various areas worldwide. A considerable body of the regional-scale study correlating the ENSO phases to hydro-climatology over low and middle latitudes provided notable evidence of statistically significant ENSO-related precipitation signals (Douglas and Englehart 1981, Schonher and Nicholson 1989, Grimm *et al.* 1998, Price *et al.* 1998, Karabörk and Kahya 2003, Lanckriet *et al.* 2014). In the mid-latitude regions, the ENSO–streamflow teleconnection has been investigated by Cayan and Peterson (1989) and Diaz and Kiladis (1993). They emphasized the impacts of the atmospheric variability over the North Pacific on streamflow in the western USA. Also, for extra-tropical teleconnections with Pacific sea-surface temperatures (SSTs), Kahya and Dracup (1994) carried out diagnostic investigations for the response of streamflow variability over the USA to extreme ENSO events. Kahya and Karabörk (2001) analysed remote forcing of the ENSO phenomenon to mid-latitude streamflow patterns in Turkey using harmonic and composite analyses, and Chiew *et al.* (1994) identified consistent seasons and coherent regions in southeast Australia, in which streamflow patterns were statistically correlated with the warm/cold phases of ENSO events. Furthermore, Chandimala and Zubair (2007) predicted seasonal streamflow variability over the Kelani River, Sri Lanka, using empirical and statistical approaches including principal component analysis. Zhang *et al.* (2007) demonstrated teleconnections between extreme ENSO phenomena and maximum streamflows of the Yangtze River basin in China using cross-wavelet analysis, while

CONTACT Jai Hong Lee june.lee@colostate.edu

Kashid *et al.* (2010) and Maity and Kashid (2010, 2011) used artificial intelligence (AI) tools with statistical techniques to investigate the climatic response of streamflow in the Mahanadi River, India, to large-scale atmospheric circulation.

In the Indian-Pacific rim countries, monsoon circulation could be considered as a climate indicator for hydro-meteorological variability. Wang *et al.* (2008) suggested a new index for monsoon activity using principal component analysis based on a comparative analysis of the various existing monsoon indices in East Asia. From the perspective of inter-annual variation of atmospheric circulation and precipitation, they emphasized that the Mei-Yu (Plum Rain) precipitation plays an essential role in quantifying monsoon intensity over East Asia. Using observational analyses and numerical climate modelling through an atmospheric general circulation model, ECHAM (v4.6), and a coupled model, POEM, Wang *et al.* (2013) revealed that a positive Western Pacific Subtropical High (WPSH)–ocean relationship can be used as a potential source of prediction skill for climate predictability; they emphasized the critical role of subtropical circulation for predicting the monsoon and tropical storm activity.

Significant correlations between large-scale climate fluctuations and hydro-meteorological variabilities over the Korean peninsula have been reported. Cha *et al.* (1999) carried out a diagnostic investigation on Korean climate variability associated with the ENSO phenomenon using large-scale gridded circulation data as well as synoptic data. They described the evolving climate characteristics over the Korean peninsula with respect to extreme ENSO phases, and pointed out positive modulation of warm and cold season precipitation by ENSO forcing. Lee and Julien (2015, 2016) employed harmonic and composite analyses to identify the dominant drivers of Korean climate fluctuations, and showed an ENSO-related climate relationship. Using correlation analysis between the tropical ENSO forcing over the Pacific Ocean and precipitation variability in the Korean peninsula, Shin (2002) showed climatic impacts of the tropical thermal forcing on hydrological extreme events including floods and droughts. Jin *et al.* (2005) categorized the Southern Oscillation Index (SOI) into five groups according to magnitude and transformed monthly precipitation data at two stations in Korea and Japan into non-exceedence probability and cubic root datasets. They showed statistically significant correlation between the categorized SOI and converted monthly precipitation data using Pearson and Kendall tests. In a study on the predictability of precipitation over the Korean peninsula, Kim *et al.* (2004) employed a downscaling super-ensemble technique based on the empirical orthogonal function (EOF) method. They showed that the winter precipitation pattern is significantly correlated with the second EOF pattern of sea level pressure (SLP) in East Asia, resulting in modulation of moist air supply from the western north Pacific. They also emphasized the intensified climate impacts of the East Asian monsoon circulation on the winter precipitation anomaly. Kang (1998) investigated the correlation of ENSO with Korean precipitation variability through multi-channel singular spectrum analysis, stressing significant correlation between ENSO and summer monsoon on a 3-year cycle. Kim and Jain (2011) quantified Korean precipitation intensity for the five major river basins through a separation analysis, associated with typhoon and non-typhoon moisture sources, and showed that the typhoon activity modulates the increase in precipitation in three of the major river basins. Also, Kim *et al.* (2012) carried out an exploratory analysis on the correlation of the Pacific Japan (PJ) pattern with typhoon activity associated with extreme precipitation variability for river basins throughout Korea; they revealed that the tropical cyclone (TC) activity is exhibited more frequently during positive PJ phase years than negative phase years.

Previous studies have mostly focused on monthly or seasonal mean precipitation. Thus, there has been less attention paid to the climatic relationship between large-scale climate fluctuations and extreme streamflow patterns. Also, the aforementioned studies mostly placed emphasis on global-scale remote CIs as a climate signal of large-scale atmospheric or air–sea coupled circulations, except for the studies by King *et al.* (2014), Klingaman *et al.* (2013) and Maity and Kashid (2010, 2011). King *et al.* (2014) examined Australian precipitation variability through EOT (empirical orthogonal teleconnection) decomposition analysis, and indicated that the first EOT modes of December precipitation show notable predictability up to several months in advance for the tropical Pacific Ocean SST and one year in advance for the Indian Ocean SST. Also, in a diagnostic study to understand the physical mechanism of the climatic impacts of large-scale climate indices on precipitation patterns in Queensland, Australia, Klingaman *et al.* (2013) identified remote and local drivers affecting the seasonal precipitation patterns using EOT decomposition with inter-annual and decadal variability. They classified large-scale climate indices into two categories: remote and local CIs. Apart from these studies, there has been little focus in the literature regarding the far-reaching climatic effects of both remote and local CIs on streamflow variability (Maity and Kashid 2010, 2011). However, climatic impacts on hydro-meteorological variables are not restricted to global-scale indices. Hence, it would be helpful to identify how both remote and local CIs have an effect on the extreme and mean streamflow patterns over East Asia. In a super-ensemble prediction analysis, Kim *et al.* (2004) found a strong and consistent climatic link between the East Asian monsoon activity and Korean precipitation variability. Visual inspection of the station location in their paper indicated that significant CI–precipitation relationships are not sufficiently identified, due to the limited station coverage (12 stations). Thus, this study is motivated to expand on previous works through a sufficient and adequate dataset.

The objectives of this study are to investigate the spatial and temporal variability of extreme and mean streamflow anomalies over the Korean peninsula using the empirical orthogonal teleconnection (EOT) technique and to identify significant climatic impacts of remote and local climate indicators on mid-latitude streamflow variability. In addition, predictability of extreme and mean streamflow patterns is examined through regression of sea-surface temperature (SST) gridded data on to the leading EOT patterns with varying lead times in terms of above- and below-normal streamflow conditions.

Data

The observational streamflow time series for this study were obtained from the Korea Annual Hydrological Report. It is important to obtain unimpaired streamflow records because dams and reservoirs often control the amount of seasonal streamflow, resulting in biased relationships with climate indices. In order to eliminate the impact of anthropogenic activities, such as regulation and diversion, only gauging stations located upstream of dams and reservoirs, or tributaries without regulation, were selected in this study. The total streamflow time series include 26 extreme events of ENSO phenomena in the period from 1962 to 2014. Stations without missing data for each season, as well as stations with more than 53 years of data, were selected for analysis. Accordingly, 60 stations out of a total of 478 stations were used, taking into account the spatio-temporal persistency, as shown in Fig. 1. In addition, extreme streamflow time series were generated as a follow-up to the recommendation of the Climate and Ocean – Variability, Predictability, and Change report.[1] The seasonal highest five consecutive daily streamflows define the extreme streamflow dataset. The seasonal extreme and mean streamflow time series were calculated for each station for the period 1962–2014. The extreme streamflow time series showed higher values than those of mean time series for northeastern and southern coastal areas in the summer. These noticeable streamflow values reflect the historical severe floods over the Korean peninsula, such as those caused by Typhoons Rusa and Maemi in 2002 and 2003, respectively, which devastated the northeastern and southern coastal areas.

For comparative analysis on the CI-related streamflow teleconnection, various CIs were used in this study. The Oceanic Niño Index (ONI), the Multivariate ENSO Index (MEI) and the Southern Oscillation Index (SOI), were employed as indicators of the extreme phase of the ENSO phenomenon considering atmospheric and oceanic fluctuations. The ONI time series are estimated using SST values in the Niño 3.4 index area (120°W to 170°W). In this study, the ONI dataset was obtained from the Climate Prediction Center (CPC) of the National Oceanic and

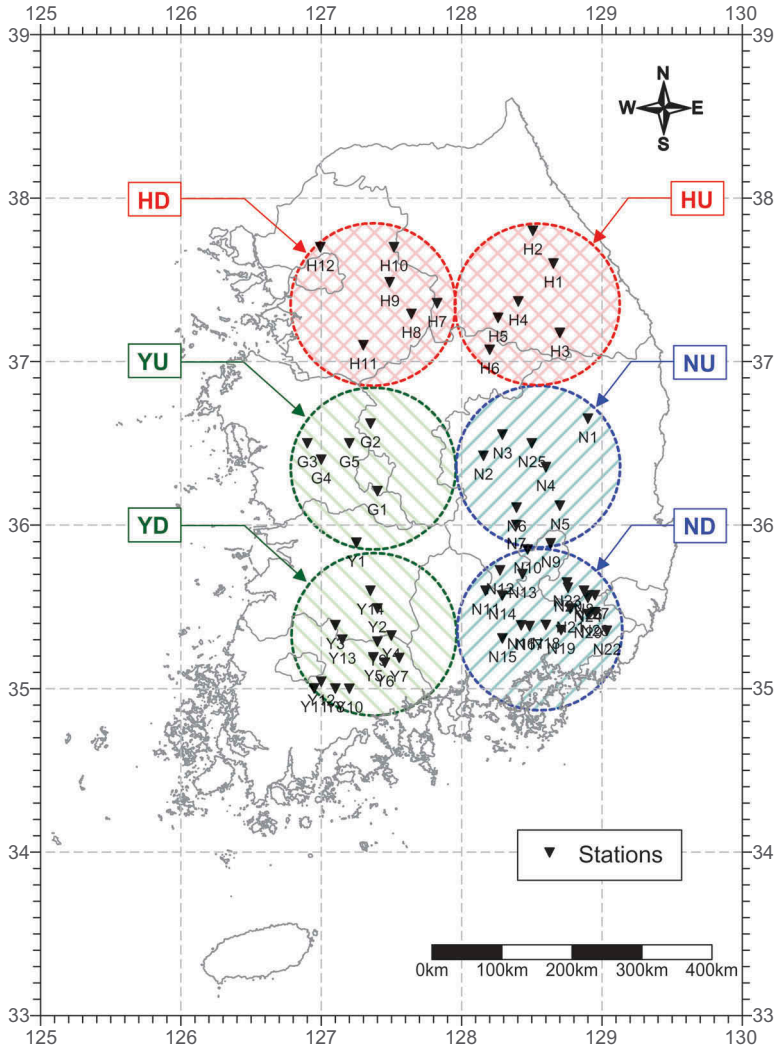

Figure 1. Stations used for streamflow indices. HU: Han River upstream; HD: Han River downstream; NU: Nakdong River upstream; ND: Nakdong River downstream; YU: Youngsan River upstream; YD: Youngsan River downstream.

[1] http://www.clivar.org/node/318.

Atmospheric Administration (NOAA).[2] The MEI is calculated using six atmospheric–ocean variables over the tropical Pacific Ocean, i.e. surface air temperature, sea-surface temperature, cloudiness fraction, zonal and meridional surface winds, and sea-level pressure. The source of the standardized bimonthly MEI time series used was the Climate Diagnostic Center (CDC).[3] The SOI, a standardized index, is estimated using mean sea-level pressure (MSLP) values between Darwin and Tahiti. In this study, the SOI time series were obtained from the NOAA-CPC.

A gridded dataset of reconstructed SSTs and a re-analysis field of atmospheric circulation were employed to investigate the teleconnection between streamflow EOT patterns and the aforementioned CIs. The Extended Reconstructed SST (ERSST.v4) was used as the reconstructed SST dataset (Huang *et al.* 2014). The ERSST time series are provided on 2.0° × 2.0° grids from 1854 to the present. The re-analysis time series of atmospheric circulation were obtained from the National Centers for Environmental Prediction – National Center for Atmospheric Research (NCEP-NCAR).[4] These time series are provided on a 2.5° × 2.5° grid basis from 1948 to the present.

As shown in Fig. 2, the western North Pacific monsoon index (WNPMI) was selected as an indicator of monsoon activity for investigating teleconnection with streamflow EOT patterns. Wang and Fan (1999) estimated WNPMI values using the difference in 850-hPa zonal winds between southern and northern index areas. In Fig. 2, U850(1) indicates the magnitude of the monsoon westerly in the area of the Indochina peninsula and the Philippines and U850(2) represents the intensity of easterly winds across the southeastern region of subtropical anticyclone over the western North Pacific. The other climate index for tropical cyclone activity, TCI, was estimated using the tracks of tropical cyclones based on the observational dataset of the IBTrACS (Knapp *et al.* 2010). These TCI time series were calculated using the number of typhoons passing through an index region near the Korean peninsula (Fig. 2).

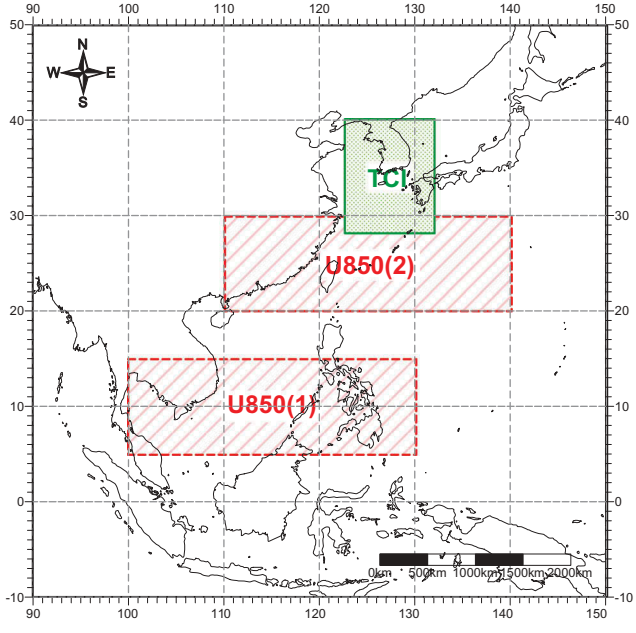

Figure 2. Map of boundaries of climate indices.

Analysis

Figure 3 outlines the overall methodology used in this study. The first step is to generate seasonal-based streamflow time series with respect to extreme and mean streamflow. The second step is to identify the spatial and temporal patterns of the extreme and mean streamflow over the Korean peninsula using the EOT method. Step 3 is to implement correlation analysis to investigate the CI-related streamflow teleconnection. Finally, Step 4 is to carry out lag-regression analysis for leading EOT streamflow patterns and tropical Pacific SST gridded data with various lag seasons for comparative interpretation of the opposite phase streamflow predictability.

EOT analysis

For the purpose of investigating spatio-temporal patterns of extreme and mean streamflow over South Korea, the empirical orthogonal teleconnection (EOT) approach was employed rather than the conventional analysis by empirical orthogonal function (EOF). The EOT method decomposes the streamflow dataset with spatio-temporal variability to a set of orthogonal components (Van den Dool *et al.* 2000). That is, the EOT technique detects a set of spatial patterns, extracts the temporal cycles, and gives an index of the importance of each pattern. The EOT approach is orthogonal in either space or time, as opposed to the empirical orthogonal function (EOF), which is orthogonal in both space and time. Thus, the advantage of using the EOT technique is that it allows the estimated patterns to be more intuitively interpreted.

The EOT-1 spatial pattern of the streamflow time series is estimated by detecting a point showing the largest sum of explained variance for all other points. Van den Dool *et al.* (2000) designated this point as the "base point (BP)". The corresponding streamflow time series of the first BP is assigned as the EOT-1 temporal pattern. The second spatial pattern of streamflow EOT time series is obtained by performing regression analysis for streamflow time series of the first BP on to the residual points to remove the impacts of the BP upon the streamflow dataset. For the reduced streamflow time series, the next BP is extracted by identifying the second point having the greatest amount of variance across the residual domain. To extract more EOT patterns in the residual domain reduced by the previous decomposition process, the reduction process is successively repeated until the optimum number of spatial and temporal patterns of a streamflow dataset is found. The following mathematical expressions of the EOT procedure are based on Van den Dool

[2]https://origin.cpc.ncep.noaa.gov/products/analysis_monitoring/ensostuff/ONI_v5.php.
[3]http://www.cdc.noaa.gov/index.html.
[4]https://www.esrl.noaa.gov/.

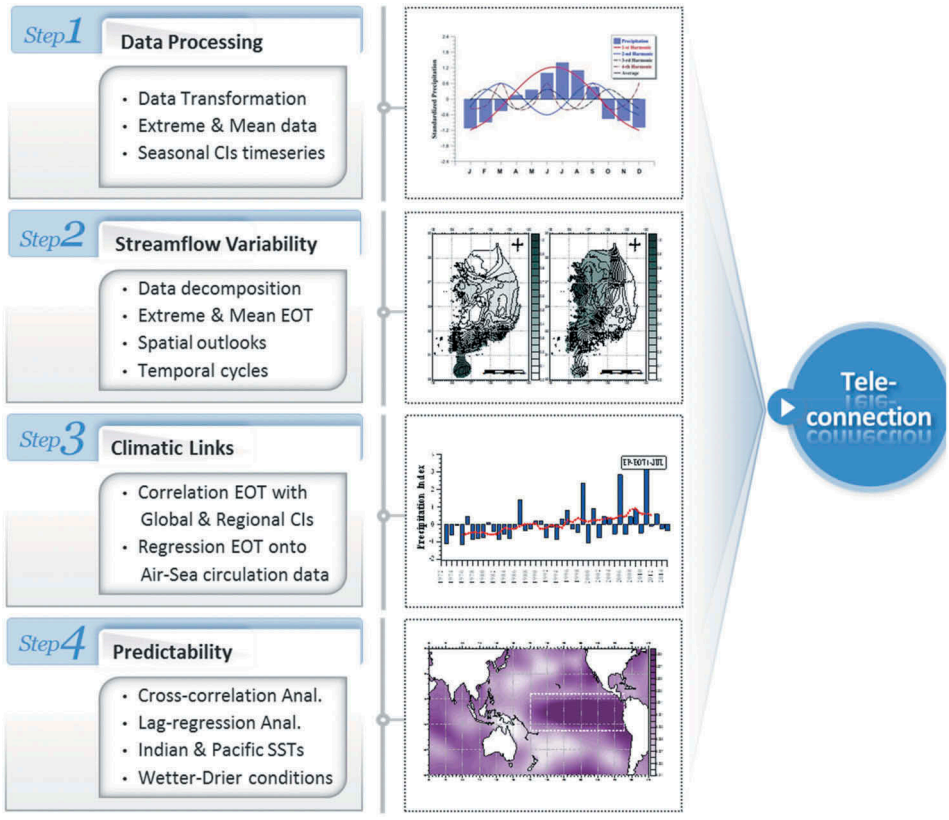

Figure 3. Flowchart of the methodology.

et al. (2000). After detecting the BP (s_{b1}) in space that explains the greatest amount of variance in the residual domain, its associated spatial mode, $e_1(s)$, is defined as the first EOT. The temporal mode, $\alpha_1(t)$, associated with EOT-1 is simply the original time series for its base point:

$$E_1(s) = \mathrm{COR}(s, s_{b1}) \frac{\mathrm{STD}(s)}{\mathrm{STD}(s_{b1})} \tag{1}$$

$$\alpha_1(t) = Q(s_{b1}, t) \tag{2}$$

where $\mathrm{COR}(s, s_{b1})$ is the temporal correlation coefficient between streamflow time series $Q(s_{b1}, t)$ at the BP and $Q(s, t)$ at all other points. Also, $\mathrm{STD}(s_{b1})$ and $\mathrm{STD}(s)$ stand for the temporal standard deviation of $Q(s_{b1}, t)$ at the BP and $Q(s, t)$ at all other points, as follows:

$$\mathrm{COR}(s, s_{b1}) = \frac{\frac{1}{n_t}\sum_{t=1}^{n_t} Q(s,t)Q(s_{b1},t)}{\mathrm{STD}(s_{b1}) \times \mathrm{STD}(s)} \tag{3}$$

$$\mathrm{STD}(s_{b1}) = \sqrt{\frac{1}{n_t}\sum_{t=1}^{n_t} Q(s_{b1},t)^2} \tag{4}$$

$$\mathrm{STD}(s) = \sqrt{\frac{1}{n_t}\sum_{t=1}^{n_t} Q(s,t)^2} \tag{5}$$

After extracting EOT-1, the data are split into two portions, in which variance is explained, $Q_e(s, t)$ and a residual, $Q_r(s, t)$, as follows:

$$Q_e(s,t) = \alpha_1(t) e_1(s) \tag{6}$$

$$Q_r(s,t) = Q(s,t) - Q_e(s,t) \tag{7}$$

After dividing the data into explained and residual portions, the procedure is repeated using the once reduced data. The point in space that explains the most variance for all other points in $Q_r(s, t)$ becomes the BP for EOT-2. The time series connected with EOT-2 is represented by the series at its BP in the once-reduced data. After removing the variance explained by EOT-2 from the dataset, the process is repeated, until all of the domain variance in the original data is explained. Thus $Q_e(s, t)$ grows at the expense of $Q_r(s, t)$, re-ordering the variance in the original data as EOT modes. The total variance (TV) in the data is expressed by:

$$\mathrm{TV} = \frac{1}{n_t n_s} \sum_{t=1}^{n_t} \sum_{s=1}^{n_s} Q(s,t)^2 \tag{8}$$

where n_t and n_s are the numbers of points in time and space, respectively. The amount of variance explained by a particular EOT is related to the proportion of its explained variance (EV) to the total domain variance (TV):

$$\mathrm{EV} = \frac{\frac{1}{n_t n_s}\sum_{t=1}^{n_t}\sum_{s=1}^{n_s} Q_e(s,t)^2}{\mathrm{TV}} \tag{9}$$

In this analysis, we used the modified EOT method revised by Smith (2004), who selected the base point using the value of explained variance over the domain-averaged time series

rather than the greatest amount of variance across all other points. As a result of the above procedure, the EOT-1 and EOT-2 were obtained for seasonal extreme and mean streamflow time series from 1962 to 2014 in order to investigate the streamflow variability in different areas of the Korean peninsula.

Correlation and regression analyses

To describe the results from the lead–lag correlation and regression analyses between various CIs and streamflow EOT patterns, correlation coefficients and regression maps were employed. To identify the climatic impacts of various CIs on extreme and mean streamflow variability across the Korean peninsula, each streamflow EOT mode was correlated with several CIs showing spatial and temporal fluctuation, e.g. ENSO, WNPMI and TCI. In particular, as a follow-up to the statistical method by King *et al.* (2014), the Spearman approach was employed using the 95% confidence level. Even though Spearman's rank test was carried out for calculating correlation coefficients, the resultant values were generally in agreement with Pearson correlation coefficients. Also, in order to examine the predictability of seasonal streamflow, the ERSST gridded dataset over the tropical Pacific Ocean was regressed on to the EOT time series with varying seasonal leads. The regression maps were plotted on 2.0° × 2.0° grids by calculating regression coefficients between leading EOT time series and all gridded global SST datasets.

Results

Variability of streamflow EOTs

Correlation coefficients for each EOT associated with the greatest amount of variance across the residual domain streamflow were mapped for each season. The values are the correlation coefficients between the streamflow EOTs at the BPs and the streamflow dataset at all other points. Each leading EOT has the largest explained variance for extreme and mean streamflow. The spatial outlooks of the BPs of the leading EOTs and correlations for each season reflect the seasonal climatic cycles combined with the impacts of mid-latitude weather systems on the Korean peninsula. The second EOT was also computed using the procedures discussed above. Figure 4 shows the resultant patterns for the leading two EOTs of summer and winter extreme and mean streamflow. Spatial patterns of the EOTs for extreme and mean streamflow vary with the seasons (Fig. 4). The locations of BPs for extreme streamflow are similar to those for mean streamflow in summer, in the upstream of the Han River basin. During winter, the BPs of extreme EOTs shift southward, but more so for the mean streamflow to the southernmost part of the Nakdong River basin. This is particularly clear in summer, shown in Fig. 4(a) and (e), and winter, in Fig. 4(c) and (g), in which the BPs of the EOTs for streamflow are plotted for the upstream area of the Han River and the downstream area of the Nakdong River, respectively. In other seasons, such as spring and autumn (not shown), three out of eight pairs of leading patterns are in the same locations for the centre of the extreme and mean leading EOTs.

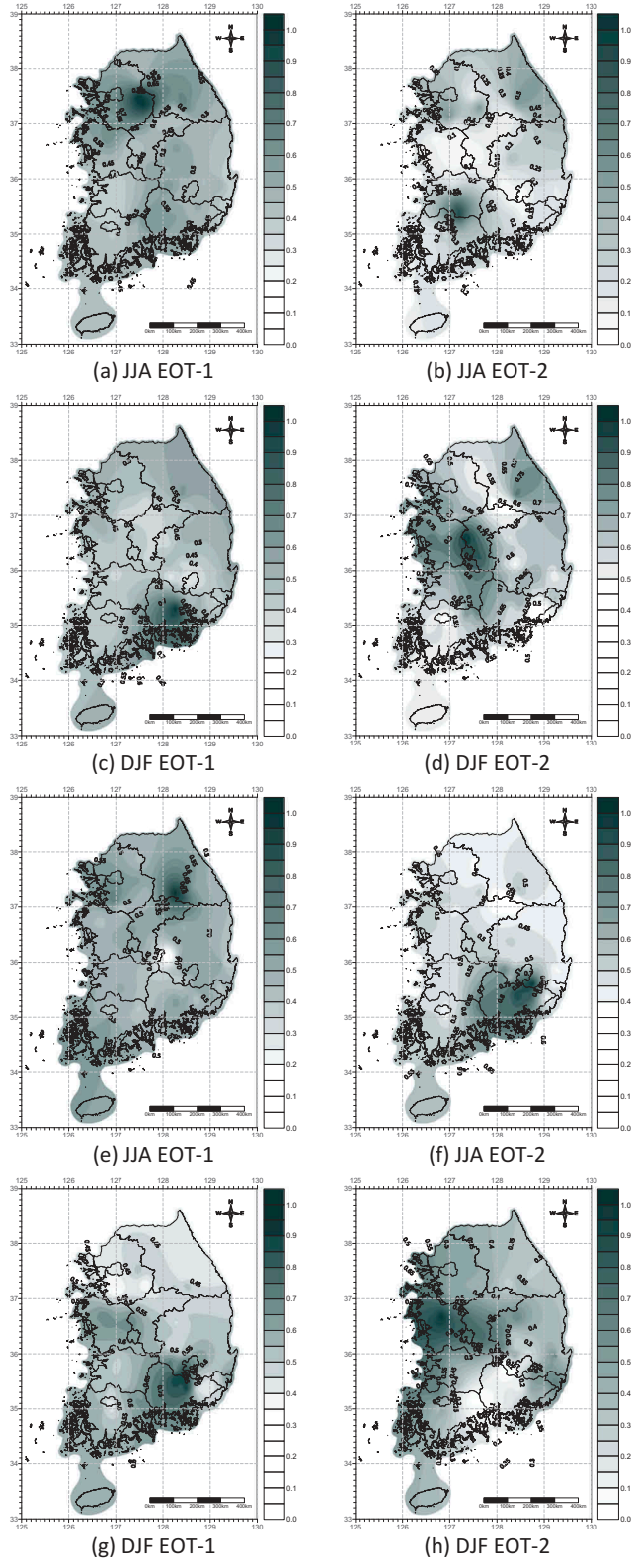

Figure 4. Maps of the locations of each EOT and the correlations between EOT time series (i.e. base point time series) and time series at all other grid points for the first and second leading EOTs of (a)–(d) extreme streamflow and (e)–(h) mean streamflow.

As shown in Table 1, the locations of the BPs indicate that out of eight extreme streamflow EOTs, i.e. two EOTs for each

Table 1. Explained variance (VE) for the two leading EOTs of seasonal extreme and mean streamflow, with the centre of the leading mode given in parentheses: HU (Han River upstream mode), HD (Han River downstream mode), NU (Nakdong River upstream mode), ND (Nakdong River downstream mode), YU (Youngsan River upstream mode), YD (Youngsan River downstream mode). IC, DC and ID denote increasing, decreasing and inter-decadal temporal cycles, respectively. NW: nationwide spatial patterns. MAM: March–April–May (spring), JJA: June–July–August (summer); SON: September–October–November (autumn); DJF: December–January–February (winter).

Mode	EOT-1				EOT-2			
	VE (%)	Spatial	Temporal	Remarks	VE (%)	Spatial	Temporal	Remarks
Extreme streamflow								
MAM	45.3	HD	-	-	21.1	NU	DC	
JJA	55.2	HD	IC	NW	19.2	YD	-	
SON	52.1	HU	-	-	17.4	NU	-	
DJF	51.4	ND	ID	NW	17.2	YU	ID	
Mean streamflow								
MAM	53.4	YD	-	-	20.2	HD	DC	
JJA	52.1	HU	IC	NW	22.4	ND	-	
SON	56.2	HU	-	NW	18.2	YD	-	
DJF	60.1	ND	ID	-	26.1	YU	-	

of the four seasons, three are identified as Han River mode, three as Nakdong River mode, and two as Youngsan River mode. For the mean streamflow, the numbers are, respectively, three, two and three. In detail, the Han River mode for extreme EOTs consists of one upstream mode and two downstream modes, according to the BPs of the leading mode, while for the mean EOTs there are two upstream modes and one downstream mode. Also, for extreme EOTS, the Nakdong River mode comprises two upstream modes and one downstream mode, and the Youngsan River mode is divided into one upstream mode and one downstream mode. For mean EOTs, the Nakdon River mode has no upstream modes and two downstream modes, and the Youngsan River mode is divided into one upstream and two downstream. The spatial structure of the EOTs for extreme and mean streamflow thus indicates an upstream mode in summer for the Han River and a downstream mode in winter for the Nakdong River. In addition, there is nationwide spatial homogeneity in leading extreme and mean streamflow modes in the summer compared to other seasons with more widespread nationwide patterns, while the only leading extreme streamflow shows nationwide spatial homogeneity in the winter. Total spatio-temporal variance associated with the first and second EOTs varies with seasons, as shown in Table 1. The values of explained variance for each extreme (mean) EOT are between 45.3% (52.1%) and 55.2% (60.1%) for leading EOTs (EOT-1), whereas those for the following EOTs decrease to about 17.2% (18.2%) at the second EOTs (EOT-2). The explained variance with the EOTs for extreme streamflow is lower than that with the leading mean EOTs for all seasons, since extreme streamflow is likely to show inhomogeneities as opposed to mean streamflow showing more consistent variation (King *et al.* 2014).

Figure 5 shows the temporal patterns for the leading EOTs of extreme and mean streamflow based on the 7-year running mean curve used by Klingaman *et al.* (2013). As shown in Table 1, four out of eight streamflow EOTs exhibit notable patterns such as increasing/decreasing trends and inter-decadal oscillations, while temporal cycles of the mean streamflow EOTs show three notable trends. The decreasing trends of these EOTs are seen for the spring (MAM), while inter-decadal variations of streamflow EOTs occur in winter (DJF). The temporal patterns of the leading EOTs represent increasing trends in summer (JJA) and inter-decadal oscillation in winter. As a general result, many EOTs have extreme and mean streamflow signals throughout the Korean peninsula with noticeable influence coverage. This indicates that the proposed climate indices in relation to large-scale circulation processes drive spatio-temporal variations of extreme and mean streamflow throughout the Korean peninsula.

Teleconnections between EOTs and climate indices

Correlation coefficients for each EOT with various CIs are shown for extreme and mean streamflow in Table 2. Additionally, regression maps for the re-analysis field of atmospheric circulation and the reconstructed SST dataset were plotted depending on each EOT pattern, as shown in Fig. 6. The regression analysis demonstrates noticeable climatic links between the two datasets, which show consistent patterns with the spatial structure commonly documented in the climate impact papers investigated.

Correlation coefficients were computed for the previously extracted EOTs and three ENSO indices (ONI, MEI, SOI). Table 2 shows that the ONI is negatively correlated with EOT-1 for extreme streamflow in summer and autumn (SON), while the leading EOT modes for winter streamflow are positively correlated with the tropical ENSO forcing. The MEI-related EOT correlations are similar to the results of the ONI time series. The SOI time series exhibit positive correlations with EOT-1 for extreme streamflow in summer and autumn, whereas the leading EOT modes for winter streamflow are negatively correlated with the ENSO indices. In spring, the ENSO-related climate signals are weaker than those for other seasons (Table 2). This reflects the fact that the far-reaching effect of the warm and cold phases of ENSO on regional climate variables is not significant in spring. Also, the correlations are weaker in warm seasons than in cold seasons because the ENSO is not in mature or decay phases. Additionally, the second EOTs exhibit significant correlations in the Han and Nakdong river basins. The results from the

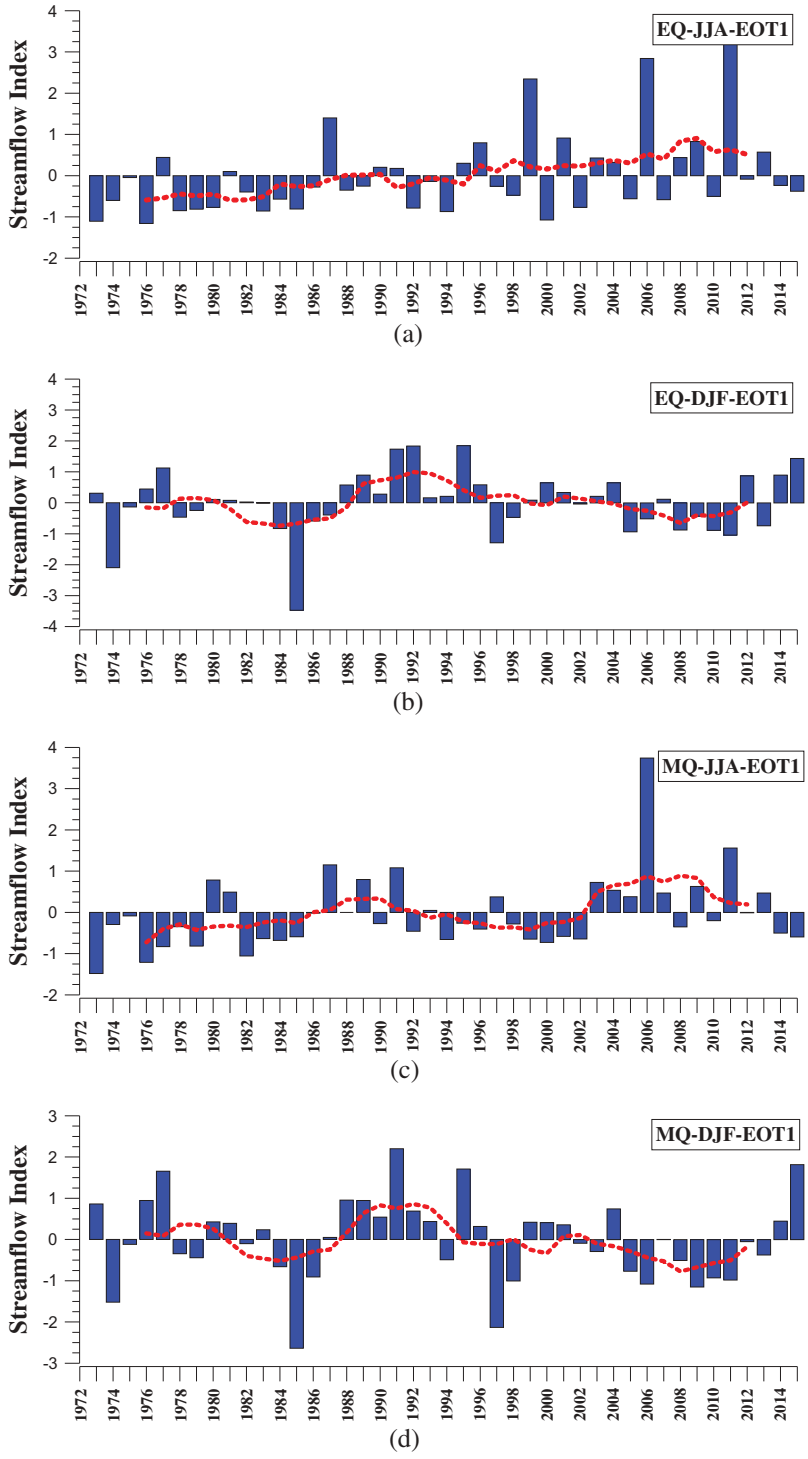

Figure 5. Annual time series (bars) and their 7-year running means (thick lines) for (a, c) the spring (JJA) EOT-1 with increasing trend and (b, d) the winter (DJF) EOT-1 with inter-decadal trend. The upper two panels are the temporal cycles for extreme streamflow and the lower two panels are those of mean streamflow.

above correlation analysis imply that the extreme phases of ENSO forcing have an effect on the variability of the extreme streamflow anomaly in the Han and Nakdong river basins. The mean streamflow EOTs also are significantly correlated with the tropical ENSO forcing. The three ENSO indices exhibit slightly lower correlations with the mean streamflow EOTs than with the EOT modes for extreme streamflow.

Climatic impacts of the ENSO forcing on the streamflow EOTs were also detected in regression fields. As shown in Fig. 6(a) and (b), highly regressed streamflow EOTs are modulated by the typical ENSO phase showing warmer than normal SST across the tropical Pacific Ocean. Warmer than normal signals for extreme and mean streamflow EOTs present the typical SST patterns of ENSO phase. Additionally, regression maps of MSLP on to the leading EOTs for winter extreme and mean streamflow (Fig. 6(c) and (d)) describe similar atmospheric circulation patterns to the tropical ENSO forcing, where low and high pressures are located in eastern

Table 2. Correlation coefficients of the two leading EOTs of seasonal extreme and mean streamflow with climate indices. ONI: Oceanic Niño Index; MEI: Multivariate ENSO Index; SOI: Southern Oscillation Index; WNPMI: Western North Pacific Monsoon Index; TCI: Tropical Cyclone Index. Bold indicates correlations that are statistically significant at the 5% level.

Mode	Extreme streamflow					Mean streamflow				
	ONI	MEI	SOI	WNP	TCI	ONI	MEI	SOI	WNP	TCI
EOT-1										
MAM	0.07	0.14	−0.08	0.21	0.24	0.05	0.05	−0.12	0.25	0.21
JJA	**−0.31**	−0.26	0.25	0.24	0.17	−0.27	**−0.34**	**0.29**	0.22	**0.28**
SON	−0.27	**−0.33**	0.24	0.09	**0.34**	−0.26	−0.27	0.25	0.10	**0.31**
DJF	**0.42**	**0.35**	**−0.41**	**−0.30**	-	**0.35**	**0.38**	−0.26	**−0.32**	-
EOT-2										
MAM	−0.03	−0.04	−0.09	−0.05	0.11	−0.03	−0.04	−0.09	−0.14	0.06
JJA	−0.15	−0.14	0.19	**−0.28**	−0.20	−0.15	**−0.28**	0.19	−0.23	−0.12
SON	**0.29**	**0.28**	−0.22	0.24	**0.31**	0.17	0.12	−0.22	**0.37**	**0.30**
DJF	0.21	0.15	−0.13	0.01	-	0.11	0.15	−0.03	0.14	-

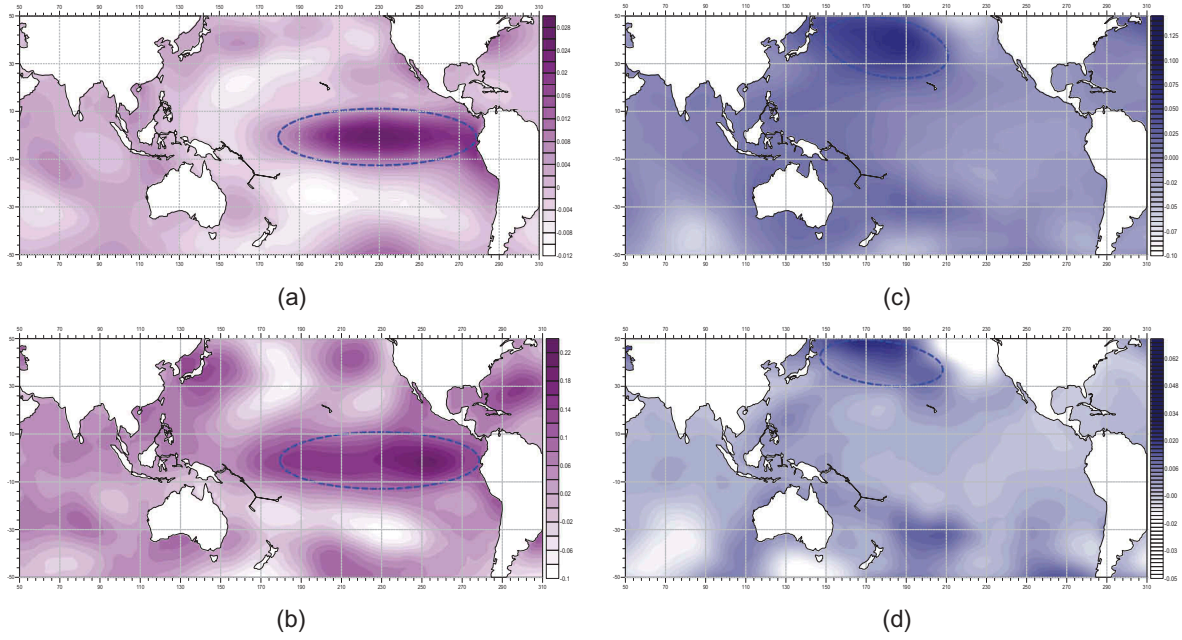

Figure 6. Maps of (a, b) SST and (c, d) MSLP regressed on to winter (DJF) EOT-1 of extreme (upper) and mean (lower) streamflow.

and western areas of the North Pacific, respectively. This phase of the atmospheric circulation, which was defined as the Pacific–East Asian teleconnection (PEA) by Wang *et al.* (2000), promotes variability of extreme and mean streamflow over the Korean peninsula during the winter season of ENSO years.

Correlation coefficients for EOTs and monsoon activity were computed using the WMPMI. As shown in Table 2, the EOTs are negatively correlated with the WMPMI time series. The positive phase of the WNPMI modulates a below-normal streamflow anomaly over the Korean peninsula. In contrast, the above-normal streamflow anomaly in winter is attributed to the negative WNPMI phase (Wang *et al.* 2000). Additionally some notable relationships between the monsoon variability and lower-order EOT time series were found in some seasons. These overall results indicate that the monsoon activity modulates the extreme streamflow over the Korean peninsula by increasing or decreasing with respect to the seasons. The mean streamflow EOTs also exhibit similar results in the correlation analysis, except for additional strong correlation between the monsoon index and the EOT-2 for mean streamflow in autumn. Monsoon variability shows higher correlation coefficients with the leading EOTs for mean streamflow than extreme streamflow EOTs.

For seasonal tropical cyclone variability, the TCI was estimated for the index area, as shown in Fig. 2. Correlation analysis was performed for the TCI time series and the leading EOTs for extreme and mean streamflow from spring to autumn. Table 2 shows that the TCI has significant correlation with two out of six extreme streamflow EOTs. This indicates that both increases and decreases of tropical cyclone events passing through the index area have an effect on the enhancement and suppression of the extreme streamflow anomaly. On the other hand, three out of six mean streamflow EOTs are significantly correlated with the TCI time series. From the findings of the correlation analysis, there are three significant positive correlations between TCI and mean streamflow EOTs, two of which are seen in the upstream area of the Han River basin. The leading EOTs for autumn streamflow show the strongest positive correlation with the TCI time series. That is, during autumn, the leading EOTs in the upstream of the Han River basin are positively correlated with tropical cyclone activity. The general findings of the above analysis are consistent with the previous findings

of Cha *et al.* (1999), who reported a significant correlation between tropical cyclones and seasonal climatic variabilities over the Korean peninsula.

Predictability of streamflow

Despite the fact that it is worthwhile to extend the understanding of the potential CI effects for streamflow variability, it is also important to improve predictability of this variability. The previously performed correlation analysis did not take into account any time lags between the EOT time series for extreme and mean streamflow and various CIs. If the various CIs applied here have a significant impact on the streamflow anomalies over South Korea, then it is worthwhile to quantify the degree of this influence by a cross-correlation analysis between the two time series. To provide not only an improved predictability of potential sources of prediction skill, but also further understanding of the far-reaching response of the CIs to the mid-latitude streamflow variability, the lead–lag correlation was quantified by correlating the seasonal EOTs for the extreme and mean streamflow with different time lag CIs that are set up from lag-0 to lag-5 on a seasonal basis. It was attempted to capture a signal period showing significant correlation of the streamflow EOTs with the CIs along the entire preceding year of the events for which streamflow patterns, CIs and the time lag are substantially associated with each other. The overall correlation coefficients were calculated at 0.05, 0.10 and 0.15 significance levels for station-based analysis for better comparison.

Cross-correlation analysis was carried out for the leading EOTs and the aforementioned three ENSO indices (ONI, MEI, SOI) with varying lead times. The EOT-1 for winter extreme streamflow has a positive correlation with the ONI from summer to winter, whereas the summer to autumn ONI time series are negatively correlated with the leading EOTs for the autumn extreme streamflow anomaly. The results of the MEI-related EOT cross-correlation analysis are similar to those of the ONI time series with the lagged signals two seasons in advance. The SOI time series from autumn to winter are negatively correlated with EOT-1 for winter extreme streamflow, while the leading EOT modes for autumn streamflow are positively correlated with the SOI time series from summer to autumn.

As shown in Table 3, significant correlation was not found in spring. This reflects that the ENSO-related streamflow signals are not significant during spring. Also, lagged correlation is stronger in the cold season than in the warm season because the ENSO phase is mature or fully developed during the cold season. The findings of the above analyses imply that the teleconnection between the tropical ENSO forcing and extreme streamflow variability over the Korean peninsula is detectable with two seasonal lags. In addition, the mean streamflow EOTs have significant lagged correlation with ENSO indices. The three ENSO indices have slightly lower correlation coefficient values with the extreme streamflow EOTs than those with the mean streamflow EOTs, but the two results indicate a similar seasonal pattern. The lagged responses of the leading EOTs for mean streamflow to the ONI, MEI and SOI indices similarly reflect those of the first EOTs for extreme streamflow.

To investigate the potential sources of predictability of the seasonal streamflow anomaly, the SST gridded dataset of ERSST.v4 was regressed on to the previously extracted EOT patterns with varying lead seasons. Figures 7 and 8 show that the winter lag-0 to lag-2 regression maps, regressing summer to winter SSTs on to winter leading EOTs, have potential predictability with positive signals, which extend to seasons prior to summer. Also, the lag regression of the SSTs on to the autumn and summer EOTs for extreme streamflow indicates notable concurrent and lagged signals. The autumn lag-1 regression, regressing

Table 3. Cross-correlation coefficients of the leading EOTs of seasonal extreme and mean streamflows with climate indices. The bold, single underlined bold, and double underlined bold indicate correlations that are statistically significant at the 0.15, 0.10 and 0.05 levels. + indicates the following year.

Mode	Seasonal CIs for extreme streamflow				Seasonal CIs for mean streamflow			
	MAM	JJA	SON	DJF	MAM	JJA	SON	DJF
Lag EOT for Oceanic Niño Index (ONI)								
MAM	0.07	-	-	-	0.05	-	-	-
JJA	0.18	**−0.31**	-	-	0.15	**−0.27**	-	-
SON	0.14	**−0.30**	**−0.27**	-	0.10	**−0.32**	**−0.26**	-
DJF	−0.07	**0.26**	**0.41**	**0.42**	−0.12	**0.26**	**0.44**	**0.35**
MAM+	**0.26**	0.20	0.23	**0.26**	0.25	0.18	0.23	0.22
JJA+	0.08	−0.12	**0.28**	−0.02	0.16	**−0.24**	0.20	−0.10
Lag EOT for Multivariate ENSO Index (MEI)								
MAM	0.14	-	-	-	0.05	-	-	-
JJA	0.21	**−0.26**	-	-	0.21	**−0.34**	-	-
SON	0.10	**−0.29**	**−0.33**	-	0.10	**−0.29**	**−0.27**	-
DJF	−0.04	**0.25**	**0.26**	**0.35**	−0.04	**0.26**	**0.29**	**0.38**
MAM+	0.16	**0.24**	0.20	**0.25**	0.16	0.21	0.19	0.22
JJA+	−0.10	−0.20	0.18	−0.12	**−0.25**	−0.20	0.18	−0.12
Lag EOT for Southern Oscillation Index (SOI)								
MAM	−0.08	-	-	-	−0.12	-	-	-
JJA	0.20	**0.25**	-	-	0.18	**0.29**	-	-
SON	−0.08	**0.29**	**0.24**	-	−0.12	**0.33**	**0.25**	-
DJF	0.16	−0.22	**−0.38**	**−0.41**	0.20	**−0.24**	**−0.39**	**−0.26**
MAM+	−0.15	−0.16	−0.23	**−0.27**	−0.19	−0.18	−0.22	**−0.24**
JJA+	0.10	0.14	0.21	0.08	0.12	0.08	0.16	0.14

SSTs from previous seasons on to autumn leading EOTs, has a notable effect on the SST-related predictability, with negative regression signals. The significant signals are exhibited until seasons prior to summer, and then diminish. However, from a closer inspection of Fig. 7 and 8,

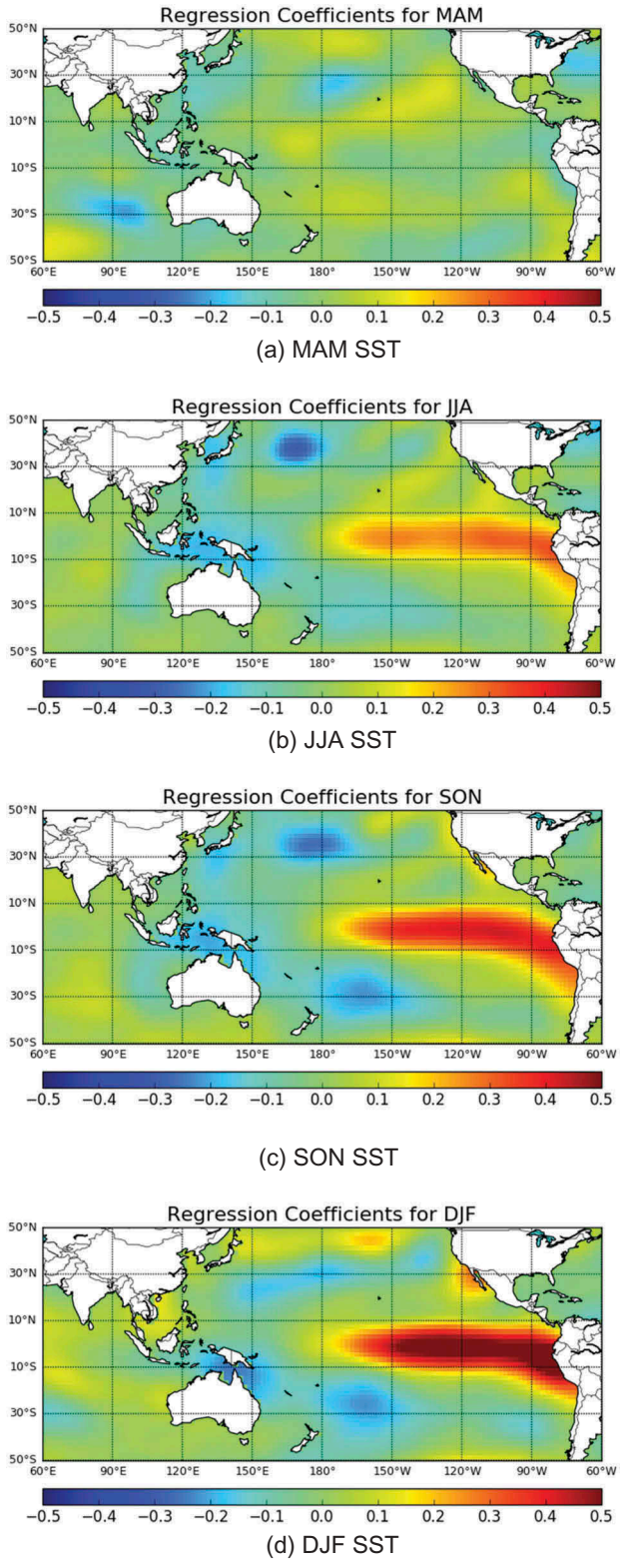

Figure 7. Maps of SSTs for each season: (a) spring (MAM), (b) summer (JJA), (c) autumn (SON) and (d) winter (DJF), regressed on to DJF extreme EOT-1.

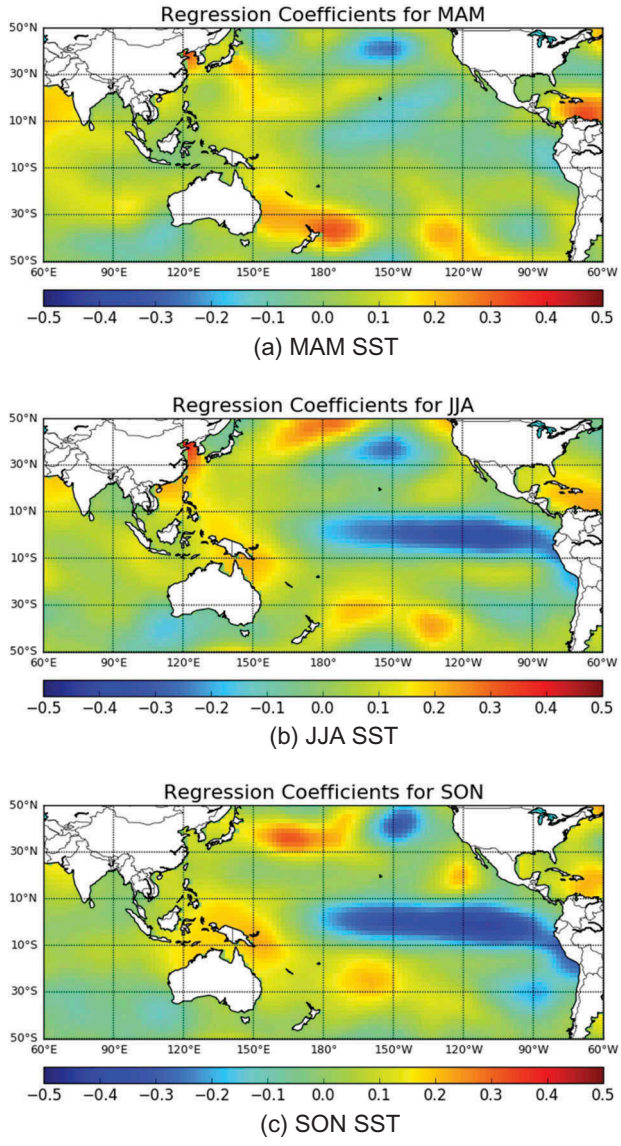

Figure 8. Maps of SSTs for each season: (a) spring (MAM), (b) summer (JJA) and (c) autumn (SON), regressed on to SON extreme EOT-1.

potential sources of predictability are not clearly detected through spring–winter SST over the Indian Ocean.

In winter, there are asymmetric patterns in the ENSO-related streamflow signals. Figure 9 describes the asymmetric tendency using the concurrent and lagged SST regression on to the winter EOTs for wetter and drier than average streamflow anomalies. The result of comparative analysis suggests that the SST-related predictabilities for above-normal streamflow are stronger than those for below-normal streamflow in winter. The SST-related predictable signals for the streamflow anomaly in spring are lower due to the weaker relationship between the SST anomaly and streamflow variability in this season. Potential predictability based on lag regression analyses extends to the EOTs for mean streamflow. The outcomes of the potential predictability analysis above provide important implications for seasonal forecasting for hydrological extreme events such as floods and droughts.

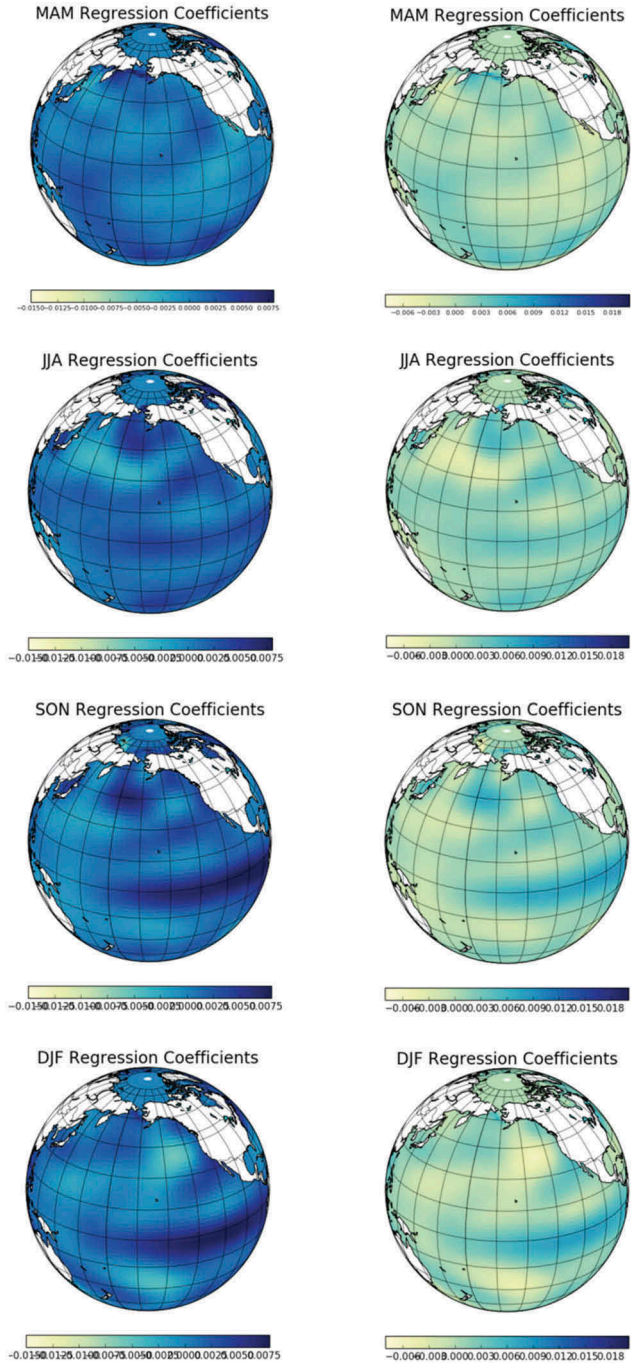

Figure 9. Maps of SSTs (from top to bottom) of spring (MAM) to winter (DJF) regressed on to DJF extreme EOT-1for wetter-than-average (left) and drier-than-average (right) extreme values only.

Discussion

The previous sections described empirical and statistical approaches for detecting a significant far-reaching effect of seasonal SST fluctuations on leading EOT patterns for extreme and mean streamflow, and showed that winter streamflow EOTs are positively correlated with the tropical Pacific thermal forcing, whereas autumn streamflow EOTs show a negative response to the air–sea coupled circulation variability over the Pacific Ocean. That is, wetter than average streamflow anomalies are observed in the winter of warm ENSO event years, while drier than average streamflow departures exhibit in the autumn. In contrast, during cold ENSO event years, winter streamflow anomalies show negative signals, whereas autumn streamflow exhibits a positive anomaly. Figure 10 describes the comparative interpretation for the opposite patterns above using the seasonal streamflow time series over the Korean peninsula. The symbols represent the standardized indices for wetter (drier) than average streamflow in winter and drier (wetter) than average streamflow in autumn of the warm (cold) ENSO event years. Distribution of the scatter plots for warm event years is concentrated on the upper left part, whereas in the cold event years, the points are distributed on the lower right side. This shows the opposite tendency of the above- and below-normal streamflow anomalies in winter and autumn of extreme event years.

What causes the anomalous streamflow over the Korean Peninsula can be explained by circulation anomalies associated with the tropical thermal forcing based on the composite difference of circulation fields. Northerly winds cut off the moisture supply from the equator towards the Korean peninsula, resulting in drier than average streamflow activity. In addition, the drier than average streamflow anomalies in autumn are attributed to the suppression of the second rainy season by a decline in typhoons and tropical storms over East Asia in the warm phase years, while wetter than average streamflow anomalies in autumn of the cold phase years are associated with the strengthening of the second rainy season caused by more frequent tropical cyclones. In contrast, during the winter season, anomalous southwesterly winds prevail over the Korean peninsula and the northwestern part of the Philippine Sea anticyclone, reflecting damping

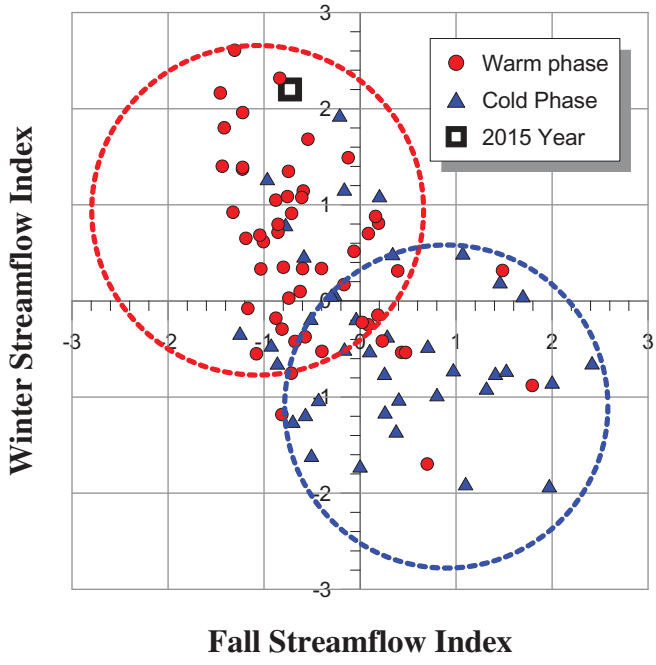

Figure 10. Comparison of standardized indices for below (above) normal streamflow in autumn and above (below) normal streamflow in winter during the warm (cold) phase of ENSO using the streamflow time series (Fall is autumn).

phases of East Asia winter monsoon or a warmer than normal winter. The anomalous southerly wind transports moist and warm air towards the Korean peninsula. A wetter than normal climate over the Korean peninsula is attributed to this northward transport.

The present findings from the empirical and statistical analyses are generally consistent with those from recent investigations for the climatic impacts of large-scale CIs on hydro-meteorological variables over the Korean peninsula. Cha *et al.* (1999) investigated climatic impacts of the tropical thermal forcing on various climate variables over the Korean peninsula, e.g. atmospheric circulation, precipitation, temperature. They suggested that extreme phases of the ENSO cycle have an effect on the seasonal variability of the precipitation anomaly with increase or decrease of its magnitude. Also, Shin (2002) found below normal precipitation anomalies in autumn during the warm phase of ENSO event years. This finding is fairly consistent with the present result of drier autumn with the ENSO-related streamflow signal season identified by the correlation and regression analyses for extreme and mean streamflow anomalies. Thus, the outcomes of this study provide additional confirmation for the previously reported climatic links between large-scale CIs and climate variation in the Korean peninsula, which describe a wetter (drier) winter in the warm (cold) event years and a drier (wetter) autumn in the extreme event years.

Summary and conclusions

In this study, an empirical approach by the EOT decomposition technique was applied to extreme and mean streamflow data to identify a climatic impact of large-scale CIs on streamflow over the Korean peninsula. In addition, potential predictability of streamflow patterns from the seasonal SST anomalies was demonstrated using correlation and regression analysis between the tropical thermal forcing and the leading EOTs.

Through the EOT process, the spatio-temporal features of extreme and mean streamflow over the Korean peninsula present an upstream mode with increasing trend during summer for the Han River and a downstream mode with inter-decadal time scales in winter for the Nakdong River. In addition, both leading extreme and mean streamflow modes show notable spatial homogeneity for the summer, with more widespread coherent streamflow patterns, while only the leading extreme EOTs show nationwide spatial homogeneity in winter. However, the leading extreme EOTs explain less variance in streamflow variability than those of mean streamflow. From the correlation analysis, the leading EOTs for extreme streamflow are negatively correlated with the ONI and MEI time series in summer and autumn, whereas the leading EOTs for winter are positively correlated with the ENSO forcing. The SOI time series exhibit positive correlations with EOT-1 for extreme streamflow in summer and autumn, while the leading EOT modes for winter streamflow are negatively correlated with the ENSO indices. The three ENSO indices exhibit slightly lower correlations with the mean streamflow EOTs than those with the EOT modes for extreme streamflow. Correlation coefficients between the leading EOTs and monsoon and tropical cyclone activities suggest that the leading EOTs for winter streamflow are negatively correlated with the monsoon indices, and the leading EOTs for autumn streamflow are positively correlated with the TCI time series. As a general result from the empirical and statistical analyses, the leading EOTs for autumn and winter extreme streamflow show the SST-related streamflow predictability one to two seasons in advance. Also, the SST-related predictability for above-normal streamflow is stronger than that for below-normal streamflow in winter.

The methodological approaches described here do not take into account the types of tropical ENSO phenomena, which are categorized into classical El Niño and El Niño Modoki according to the location of peak SST anomalies. Further investigation of the climatic responses of the two types of ENSO forcing on hydro-meteorological variables in the tropics and extra-tropics needs to be performed in more detail. The overall findings of this study stress the importance of extending the remote climatic impacts of the tropical thermal forcing to South Korean streamflow and motivate additional comparative analysis on how the two types of ENSO forcing may be influencing mid-latitude streamflow variability.

Disclosure statement

No potential conflict of interest was reported by the authors.

References

Cayan, D.R. and Peterson, D.H., 1989. The influence of North Pacific atmospheric circulation on streamflow in the West, in Aspects of climate variability in the Pacific and the Western Americas. *American Geophysical Union, Monographs*, 55, 375–397.

Cha, E.J., Jhun, J.G., and Chung, H.S., 1999. A study on characteristics of climate in South Korea for El Niño/La Niña Years. *Journal of the Korean Meteorological Society*, 35 (1), 99–117.

Chandimala, J. and Zubair, L., 2007. Predictability of streamflow and rainfall based on ENSO for water resources management in Sri Lanka. *Journal of Hydrology*, 335, 303–312. doi:10.1016/j.jhydrol.2006.11.024

Chiew, F.H.S., *et al.*, 1994. El Niño/Southern Oscillation and the streamflow patterns in south-east Australia. Civil Engineering Transactions. *Institution of Engineers, Australia*, CE36 (4), 285–291.

Diaz, H.F. and Kiladis, G.N., 1993. El Niño/Southern Oscillation and streamflow in the western United States. *In*: H.F. Diaz and V. Markgraf, eds. *El Niño: historical and paleoclimatic aspects of the Southern Oscillation*. Cambridge, UK: Cambridge University Press, 8–28.

Douglas, A.E. and Englehart, P.J., 1981. On a statistical relationship between autumn rainfall in the central equatorial pacific and subsequent winter precipitation in Florida. *Monthly Weather Review*, 109, 2377–2382. doi:10.1175/1520-0493(1981)109<2377:OASRBA>2.0.CO;2

Grimm, A.M., Ferraz, S.E.T., and Gomes, J., 1998. Precipitation anomalies in Southern Brazil associated with El Niño and La Niña events. *Journal of Climate*, 11, 2863–2880. doi:10.1175/1520-0442(1998)011<2863:PAISBA>2.0.CO;2

Huang, B., *et al.*, 2014. Extended Reconstructed Sea Surface Temperature version 4 (ERSST.v4): part I. Upgrades and intercomparisons. *Journal of Climate*. doi:10.1175/JCLI-D-14-00006.1

Jin, Y.H., *et al*., 2005. Quantitative relationship between SOI and observed precipitation in southern Korea and Japan by nonparametric approaches. *Journal of Hydrology*, 301, 54–65. doi:10.1016/j.jhydrol.2004.06.026

Kahya, E. and Dracup, J.A., 1994. The influences of Type 1 El Niño and La Niña events on streamflows in the Pacific southwest of the United States. *Journal of Climate*, 7, 965–976. doi:10.1175/1520-0442(1994)007<0965:TIOTEN>2.0.CO;2

Kahya, E. and Karabörk, M.C., 2001. The analysis of El Niño and La Niña signals in streamflows of Turkey. *International Journal of Climatology*, 21 (10), 1231–1250. doi:10.1002/joc.663

Kang, I.S., 1998. Relationship between El-Niño and Korean climate variability. *Journal of the Korean Meteorological Society*, 34 (3), 390–396.

Karabörk, M.Ç. and Kahya, E., 2003. The teleconnections between extreme phases of Southern Oscillation and precipitation patterns over Turkey. *International Journal of Climatology*, 23, 1607–1625. doi:10.1002/joc.958

Kashid, S.S., Ghosh, S., and Maity, R., 2010. Streamflow prediction using multi-site rainfall obtained from hydroclimatic teleconnection. *Journal of Hydrology*, 395, 23–38. doi:10.1016/j.jhydrol.2010.10.004

Kiladis, G.N. and Diaz, H.F., 1989. Global climatic anomalies associated with extremes in the Southern Oscillation. *Journal of Climate*, 2, 1069–1090. doi:10.1175/1520-0442(1989)002<1069:GCAAWE>2.0.CO;2

Kim, J.S. and Jain, S., 2011. Precipitation trends over the Korean peninsula: typhoon-induced changes and a typology for characterizing climate-related risk. *Environmental Research Letters*, 6, 034033. doi:10.1088/1748-9326/6/3/034033

Kim, J.S., Li, R.C.Y., and Zhou, W., 2012. Effects of the Pacific-Japan teleconnection pattern on tropical cyclone activity and extreme precipitation events over the Korean Peninsula. *Journal of Geophysical Research*, 117, D18109. doi:10.1029/2012JD017677

Kim, M.K., *et al*., 2004. Super ensemble prediction of regional precipitation over Korea. *International Journal of Climatology*, 24, 777–790. doi:10.1002/joc.1029

King, A.D., *et al*., 2014. Extreme rainfall variability in Australia: patterns, drivers, and predictability. *Journal of Climate*, 27, 6035–6050. doi:10.1175/JCLI-D-13-00715.1

Klingaman, N.P., Woolnough, S.J., and Syktus, J., 2013. On the drivers of inter-annual and decadal rainfall variability in Queensland, Australia. *International Journal of Climatology*, 33, 2413–2430. doi:10.1002/joc.2013.33.issue-10

Knapp, K.R., *et al*., 2010. The International Best Track Archive for Climate Stewardship (IBTrACS): unifying tropical cyclone besttrack data. *Bulletin of the American Meteorological Society*, 91, 363–376. doi:10.1175/2009BAMS2755.1

Lanckriet, S., *et al*., 2014. Droughts related to quasi-global oscillations: a diagnostic teleconnection analysis in North Ethiopia. *International Journal of Climatology*, 35 (7), 1534–1542. doi:10.1002/joc.4074

Lee, E.J., Jhun, J.G., and Park, C.K., 2005. Remote connection of the northeast Asian summer rainfall revealed by a newly defined monsoon index. *Journal of Climate*, 18, 4381–4393. doi:10.1175/JCLI3545.1

Lee, J.H. and Julien, P.Y., 2015. ENSO impacts on temperature over South Korea. *International Journal of Climatology*, 10, 1002/4581.

Lee, J.H. and Julien, P.Y., 2016. Teleconnections of the ENSO and South Korean precipitation patterns. *Journal of Hydrology*, 534, 237–250. doi:10.1016/j.jhydrol.2016.01.011

Maity, R. and Kashid, S.S., 2010. Short-term basin-scale streamflow forecasting using large-scale coupled atmospheric oceanic circulation and local outgoing longwave radiation. *Journal of Hydrometeorology*, 11 (2), 370–387. doi:10.1175/2009JHM1171.1

Maity, R. and Kashid, S.S., 2011. Importance analysis of local and global climate inputs for basin-scale streamflow prediction. *Water Resources Research*, 47 (11), W11504. doi:10.1029/2010WR009742

Price, C., *et al*., 1998. A possible link between El Niño and precipitation in Israel. *Geophysical Research Letters*, 25, 3963–3966. doi:10.1029/1998GL900098

Ropelewski, C.F. and Halpert, M.S., 1986. North American precipitation and temperature patterns associated with El-Niño-Southern oscillation (ENSO). *Monthly Weather Review*, 114, 2165–2352. doi:10.1175/1520-0493(1986)114<2352:NAPATP>2.0.CO;2

Ropelewski, C.F. and Halpert, M.S., 1989. Precipitation patterns associated with the high index phase of the southern oscillation. *Journal of Climate*, 2, 268–284. doi:10.1175/1520-0442(1989)002<0268:PPAWTH>2.0.CO;2

Schonher, T. and Nicholson, S.E., 1989. The relationship between California rainfall and ENSO events. *Journal of Climate*, 2, 1258–1269. doi:10.1175/1520-0442(1989)002<1258:TRBCRA>2.0.CO;2

Shin, H.S., 2002. Do El Niño and La Niña have influences on South Korean hydrologic properties? *In*: *Proceedings of the 2002 Annual Conference Japan Society of Hydrology and Water Resources*, Japan, 276–282.

Smith, I.N., 2004. An assessment of recent trends in Australian rainfall. *Australian Meteorolgy Magazine*, 53, 163–173.

Van den Dool, H.M., Saha, S., and Johansson, Å., 2000. Empirical orthogonal teleconnections. *Journal of Climate*, 13, 1421–1435. doi:10.1175/1520-0442(2000)013<1421:EOT>2.0.CO;2

Walker, G.T., 1923. Correlation in seasonal variations of weather, VIII. A preliminary study of world weather. *Memoirs of the India Meteorological Department*, 24 (4), 75–131.

Walker, G.T. and Bliss, E.W., 1932. World weather V. *Memoirs of the Royal Meteorological Society*, 4 (36), 53–84.

Wang, B. and Fan, Z., 1999. Choice of South Asian summer monsoon indices. *Bulletin of the American Meteorological Society*, 80, 629–638. doi:10.1175/1520-0477(1999)080<0629:COSASM>2.0.CO;2

Wang, B., Wu, R., and Fu, X., 2000. Pacific–east Asian teleconnection: how does ENSO affect East Asian climate. *Journal of Climate*, 13, 1517–1536. doi:10.1175/1520-0442(2000)013<1517:PEATHD>2.0.CO;2

Wang, B., *et al*., 2008. How to measure the strength of the East Asian Summer Monsoon. *Journal of Climate*, 1175, 4449–4463.

Wang, B., Xiang, B., and Lee, J., 2013. Subtropical high predictability establishes a promising way for monsoon and tropical storm predictions. *Proceedings of the National Academy of Sciences, USA*, 110, 2718–2722. doi:10.1073/pnas.1214626110

Zhang, Q., *et al*., 2007. Possible influence of ENSO on annual maximum streamflow of the Yangtze River, China. *Journal of Hydrology*, 333, 265–274. doi:10.1016/j.jhydrol.2006.08.010